Journal of Materials Chemistry A

Accepted Manuscript

This article can be cited before page numbers have been issued, to do this please use: M. Nam, J. Yoo, Y. Park, H. Y. Noh, Y. Park, J. Cho, J. A. Kim, J. Kim, H. H. Lee, R. Chang and D. Ko, *J. Mater. Chem. A*, 2019, DOI: 10.1039/C9TA00382G.

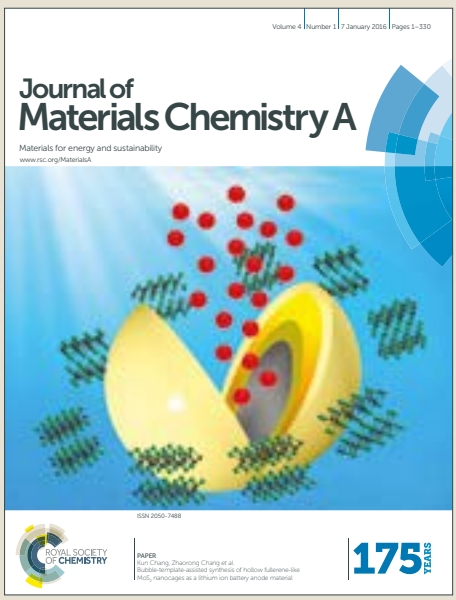

ROYAL SOCIETY OF CHEMISTRY

rsc.li/materials-a

View Article Online
DOI: 10.1039/C9TA00382G

Journal of Materials Chemistry A

PAPER

Ternary blend organic solar cells with improved morphological stability

Received 00th January 20xx,
Accepted 00th January 20xx

DOI: 10.1039/x0xx00000x

www.rsc.org/

Minwoo Nam,‡[a] Jaehong Yoo,‡[a] Yunjae Park,‡[b] Hye Yeon Noh,[a] Yongkook Park,[a] Junhee Cho,[a] Jung-A Kim,[a] Jehan Kim,[c] Hyun Hwi Lee,[c] Rakwoo Chang*[b] and Doo-Hyun Ko*[a]

Long-term stability of organic blends is a key factor for the practical use of organic solar cells (OSCs) in commercial fields. Here, we report the strategic incorporation of non-fullerene small molecules in polymer:fullerene blends to obtain ternary OSCs with improved efficiency and extended lifetimes. Non-fullerene small molecules employed in the polymer:fullerene blend successfully increased the photon-to-current conversion process as an efficient charge cascade acceptor. A combination of theoretical simulations and experimental measurements revealed that aggregation of meta-stable fullerene molecules was significantly alleviated in the ternary blend, thereby preventing an unintentional increase in the threshold for charge transfer during operation. Thus, the ternary OSCs could exhibit highly extended lifetimes with improved morphological stability and better resistance to performance decay under harsh real operational conditions compared to their binary counterparts. Combined with its high efficiency and improved device lifetimes, the high tolerance to the ternary blend thickness offers promise for commercially acceptable ternary OSCs fabricated by a printing process.

Introduction

Bulk heterojunction (BHJ) organic solar cells (OSCs) are of great interest in academic and industrial fields as solution-processable, cost-effective, mechanically flexible, and large-scale next-generation energy platforms. A great deal of research effort has been devoted to increasing power conversion efficiency (PCE) so that it approaches a commercially acceptable level. These efforts have included new material development,[1] solvent additives,[2] device interface engineering,[3] and multi-component (ternary or quaternary) BHJ approaches.[4,5] On the downside, the long-term stability of OSCs remains a critical issue, and it is imperative to further understand and solve the current lifetime limitation factors to ensure the commercial viability of OSCs. One of the important limiting factors involves meta-stable organic blends that reduce the overall device performance under real operational conditions.[6] For instance, [6,6]-phenyl-C_{71}-butyric acid methyl ester ($PC_{70}BM$) readily aggregates due to its thermodynamic instability accompanied by a reduction in donor-acceptor (D-A) interfacial areas and an undesirable increase in the percolation threshold for charge transfer.[7,8]

One promising approach to improve the morphological stability of BHJs involves the design and synthesis of novel acceptor materials that are resistant to thermally induced morphology changes. Recent studies have claimed better stability of non-fullerene acceptors over conventional fullerene derivatives under thermal stress.[9,10] In addition, non-fullerene acceptors, such as the ITIC family (based on an indacenodithieno[3,2-b]-thiophene core), provide promising PCEs of over 10%, even exceeding that of conventional $PC_{70}BM$-based devices, resulting from their advantages of strong absorptivity in the visible region and tunable energy levels (by chemical modification), both of which can be readily optimized depending on the donor material.[11,12] To the best of our knowledge, very few reports successfully pursued the morphology evolution of non-fullerene acceptors or demonstrated their excellent stability under real operational conditions on a long time scale. As an alternative approach to prolong the lifetime of OSCs, the facile incorporation of additional components preserves the optimized morphology of the pristine BHJs, which involves non-crystalline fullerenes, chemically cross-linkable fullerenes, or fullerene nucleating agents.[13-16] In a previous study, we successfully improved the morphological stability and extended the lifetime of OSCs via incorporation of additional donors or acceptors to make multi-component BHJ systems.[5] This success was attributed to the excellent preservation of the optimized morphology of the pristine active layer under high temperature conditions, resulting from kinetic and thermodynamic effects between the components. This scheme is desirable in that it can lock in the

[a] Department of Applied Chemistry, Kyung Hee University, Yongin, Gyeonggi 17104, Republic of Korea. *E-mail: dhko@khu.ac.kr
[b] Department of Chemistry, Kwangwoon University, Seoul 01897, Republic of Korea. *E-mail: rchang@kw.ac.kr
[c] Pohang Accelerator Laboratory, Pohang, Gyeongbuk 37673, Republic of Korea.
† Electronic Supplementary Information (ESI) available: Additional details and supplementary results. See DOI: 10.1039/x0xx00000x
‡ These authors contributed equally to this work.

View Article Online
DOI: 10.1039/C9TA02030C

nanomorphology of pristine films by commercially available donor or acceptor materials without requiring new material development, sacrificing the facile processing, or deteriorating the initial efficiency.

In this study, we demonstrate a ternary BHJ layer involving a non-fullerene acceptor for high-efficiency and highly stable OSC applications. Ternary OSCs with experimentally optimized compositions exhibited better charge separation and transport through cascade energy levels and optimized blend morphology with combined benefits of fullerene ($PC_{70}BM$) and non-fullerene (3,9-bis(2-methylene-(3-(1,1-dicyanomethylene)-indanone))-5,5,11,11-tetrakis(5-hexylthienyl)-dithieno[2,3-d:2',3'-d']-s-indaceno[1,2-b:5,6-b']dithiophene, ITIC-Th) acceptors. This gave an increased PCE of ~9.44% for the ternary OSC compared with ~7.95% for the $PC_{70}BM$ binary OSC and ~7.55% for the ITIC-Th binary OSC. A combination of theoretical and experimental analyses showed that the ternary blend can benefit from improved morphological stability with significantly suppressed domain growth and phase separation between components during operation. As a consequence, the estimated device lifetime of the ternary OSC was notably increased with better morphological stability under harsh thermal stress over its binary counterpart. For instance, a ternary OSC retained more than 50% of its high initial PCE after one year of operation at 60 °C, and the PCE value surpassed that of conventional $PC_{70}BM$-based binary OSC only after one week of operation. In addition to the improved efficiency and stability, the high tolerance to the active layer thickness further opens new possibilities of printable ternary BHJ OSCs employing non-fullerene acceptors.

Results and discussion

Ternary OSC optimization

Figs. 1a and b show the chemical structures and energy levels of poly[4,8-bis(5-(2-ethylhexyl)thiophen-2-yl)benzo[1,2-b;4,5-b']dithiophene-2,6-diyl-alt-(4-(2-ethylhexyl)-3-fluorothieno[3,4-b]thiophene-)-2-carboxylate-2-6-diyl)] (PTB7-Th) as a donor (D), $PC_{70}BM$ as a host acceptor (A_1), and ITIC-Th as a guest acceptor (A_2) used in this study to form ternary BHJs. ITIC-Th is a non-fullerene small molecule based on an indacenodithieno[3,2-*b*]-thiophene core and thienyl side-chains, distinctive from the isotropic structure of the $PC_{70}BM$.[10,11] Because of the similar bandgap between PTB7-Th and ITIC-Th, their absorption profiles mostly overlap. As a consequence, $PC_{70}BM$ provides complementary absorption to PTB7-Th and ITIC-Th in ternary blends with prominent light harvesting at short wavelengths (Fig. 1c), and the absorption properties of the ternary BHJs rely on the blending ratios between two acceptors (Fig. S1, ESI†). From the intermediate energy levels of ITIC-Th between PTB7-Th and $PC_{70}BM$, we would expect efficient charge transfer between three components under the cascade energy levels. The device using a $PC_{70}BM$:ITIC-Th blend showed a short-circuit current density (J_{SC}) of 0.205 $mAcm^{-2}$, which was higher than the 0.171 and 0.180 $mAcm^{-2}$ observed for the devices based on pure $PC_{70}BM$ film and pure ITIC-Th film, respectively (Fig. 1d). The photoluminescence (PL) intensity of ITIC-Th quenched after incorporating $PC_{70}BM$ (Fig. S2, ESI†). These signified efficient charge transfer between ITIC-Th and $PC_{70}BM$, which facilitated the charge generation processes in the overall ternary device.[17,18]

Fig. 2a compares the current density-voltage (*J*–*V*) characteristics of the devices with varying ITIC-Th content without any solvent additives. The ratio between the two acceptors in the blends was intentionally controlled to determine the optimal ternary OSCs, while the donor:acceptor ratio was fixed to be 1:1.5, which is the optimum protocol based on previous reports.[1,19] All ternary blend devices outperformed both kinds of binary references, and the ternary device containing 40% ITIC-Th achieved the highest PCE of 8.91% out of the devices (refer to Fig. S3, Fig. S4, and Table S1, ESI†). Then, we incorporated a solvent additive, 1-chloronaphthalene (CN), to further improve the device performance. We adopted CN as an additive rather than the widely known 1,8-diiodooctane (DIO), which negatively influenced the morphology and photovoltaic performance of ITIC-Th (Fig. S5, ESI†). As shown in Fig. 2b, the PCE of the $PC_{70}BM$-based binary OSCs increased considerably after incorporating CN with a peak at 3 vol% (from 5.22% to 8.32%), while the addition of CN deteriorated the PCE of binary OSCs based on ITIC-Th (from 8.44% to 7.08%) (refer to all photovoltaic parameters in Fig. S6, ESI†). It was notable that the ternary OSC (ITIC-Th 40%) exhibited higher PCEs over the binary devices regardless of the CN vol%. The PCE increased with incorporating CNs with a peak at CN of 2 vol% (from 8.91% to 9.44%), but a further increase to 3 vol% rather reduced the PCE to 9.21%. Fig. 2c arranges the *J*–*V* characteristics of three kinds of devices, namely PTB7-Th:$PC_{70}BM$ (1:1.5) containing 2 vol% CN with a PCE of 7.95% ($PC_{70}BM$ binary OSC), PTB7-Th:ITIC-Th (1:1.5) containing 2 vol% CN with a PCE of 7.55% (ITIC-Th binary OSC), and PTB7-Th:$PC_{70}BM$:ITIC-Th (1:0.9:0.6) with 2 vol% CN (ternary OSC). The three devices with the same concentration of CN will be discussed to provide a fair comparison in the morphology analysis.

The J_{SC} values matched those calculated from the external quantum efficiency (EQE) spectra (Fig. 2d). We found the combined contributions of $PC_{70}BM$ and ITIC-Th to the EQE profile in the ternary OSC to compensate the limited absorption of each acceptor material. For instance, the EQE enhancement of the ternary OSC relative to the ITIC-Th binary was prominent in the short wavelength region centred at 450 nm (blue dotted line), while the EQE enhancement relative to the $PC_{70}BM$ binary was observed mainly at around 680 nm (black dotted line). In particular, a significant increase in the EQE was obtained beyond 550 nm compared with both binary references, which corresponds to the main absorption area of PTB7-Th and ITIC-Th. This indicates successful transfer of photo-generated electrons from PTB7-Th and/or ITIC-Th to $PC_{70}BM$ with three possible routes (from PTB7-Th to $PC_{70}BM$,

View Article Online
DOI: 10.1039/C9TA00782C

from PTB7-Th to ITIC-Th and then to $PC_{70}BM$, and from ITIC-Th to $PC_{70}BM$).

To evaluate the charge transfer properties of the blends in more detail, we compared the exciton dissociation probability (*P(E,T)*) between the devices using photocurrent density-effective voltage (J_{ph}–V_{eff}) characteristics in Fig. 2e. The *P(E,T)* determined by normalizing J_{ph} with the saturation current density (J_{sat}) under the short condition was 96.87% for the ternary OSC, which surpasses 91.02% and 94.52% observed for the $PC_{70}BM$ and ITIC-Th references, respectively, implying the improved exciton dissociation yield in the ternary OSC.[20-22] On the contrary, the maximum exciton generation rate (G_{max}) of 1.25×10^{28} $m^{-3}s^{-1}$ for the ternary OSC was lower than 1.36×10^{28} $m^{-3}s^{-1}$ for the $PC_{70}BM$ reference ($J_{sat} = qLG_{max}$, where q is elementary charge and L is the thickness of the active layer).[20-22] This indicates that an absorption increase is not the origin of the J_{SC} enhancement due to the absorption overlap between PTB7-Th and ITIC-Th. Then, the electron mobility of the devices was obtained by using the space charge-limited current (SCLC) method (Fig. 2f).[23] The electron mobility of the ternary OSC (1.02×10^{-3} $cm^2V^{-1}s^{-1}$) was 2.54-fold and 1.95-fold higher than that of the $PC_{70}BM$ (4.02×10^{-4} $cm^2V^{-1}s^{-1}$) and ITIC-Th (5.23×10^{-4} $cm^2V^{-1}s^{-1}$) references, respectively. The high electron mobility ensures more effective charge transport in the ternary OSC compared with the binary OSCs. We found no significant difference in recombination properties between the devices. For instance, Fig. S7 (ESI†) shows a linear power-law dependence of J_{SC} on the light intensity in logarithmic coordinates: $J_{SC} \propto P_{light}{}^{\alpha}$, where α close to 1 indicates weak bimolecular recombination in the OSC.[24] The J_{SC} of OSCs was nearly independent on the light intensity with the α of almost 1, which signifies that the recombination property remained nearly similar between the OSCs. Taken together, ITIC-Th facilitates exciton dissociation and charge transport between the PTB7-Th and $PC_{70}BM$ as a charge cascade material without generating additional recombination centers in the ternary BHJ layer.

It should be noted that we found almost constant recombination properties and PCEs in the ternary OSC while varying the active layer thickness from 105 to 255 nm (Fig. S8, ESI†). For practical applications of OSCs, it is important for the system to tolerate variations in the active layer thickness, since it is difficult to fabricate uniform films of ~100 nm thickness using industrial solution techniques such as large-area printing.[25] Therefore, the ternary approach can provide a feasible and effective way for fabricating high-efficiency OSCs compatible with a large-area printing process.

Ternary blend morphology

The nanoscale morphological features of blends were examined using atomic force microscopy (AFM). As shown in Fig. 3, the $PC_{70}BM$ blend has small domains with a smooth surface and a small root mean square (RMS) roughness of 1.05 nm (Figs. 3a and d), while the ITIC-Th blend showed relatively larger domains and a rough film surface with a larger RMS roughness of 8.54 nm (Figs. 3b and e). This agreed with the previous reports, in which ITIC-Th has a larger domain size than $PC_{70}BM$.[26-28] The ternary blend showed combined morphological features of $PC_{70}BM$ and ITIC-Th without severe aggregates between the components, and the RMS roughness of 2.11 nm was indeed between those of the binary references (Figs. 3c and f). Such morphology formation could enable the combined contributions of $PC_{70}BM$ (complementary absorption to other components and large interfacial junctions) and ITIC-Th (high charge dissociation and transport yields). Therefore, we determined that the enhanced optoelectronic properties in the ternary OSC were accompanied by improved nanomorphology and well-assembled charge pathways in the ternary blend.

However, meta-stable organic blends evolve with time during operation (e.g., aggregation of $PC_{70}BM$) accompanying phase separation of components and a severe reduction in charge transfer yields. Thus, preserving the optimized morphology of the pristine BHJs by arresting the morphological mutation of $PC_{70}BM$ is a critical issue in OSCs for their longevity and commercial viability. We investigated the time-dependent domain growth of blends obtained from grazing-incidence small-angle X-ray scattering (GISAXS) analysis, which can be used to interpret the domain sizes of the BHJ nanostructures. Fig. 4a compares the time-dependent variations in domain size between $PC_{70}BM$ and the $PC_{70}BM$:ITIC-Th alloy under accelerated mutation conditions at an elevated temperature of 60 °C, which is within the real operational temperature range.[29] Fig. S9 (ESI†) shows the corresponding 2D GISAXS patterns. Nanoscale overall domain sizes of the as-prepared samples were 19.5 and 32.8 nm for the $PC_{70}BM$ and $PC_{70}BM$:ITIC-Th alloy, respectively, which accorded well with previous reports.[26-28] During operation at 60 °C, the $PC_{70}BM$ blend showed continuous growth of its aggregates with a considerable increase factor of 58.5% (domain growth rate of 1.63 nm/day), while the ternary blend exhibited a significantly suppressed increase factor of 4.9% (0.23 nm/day). This suggests that the introduction of ITIC-Th could effectively preserve the optimized morphology of the pristine ternary BHJs by retarding the aggregation behaviour of $PC_{70}BM$ under thermal stress.

Then, we evaluated *P(E,T)* values of devices for different annealing times at 60 °C since charge transfer is one of the critical factors that is strongly governed by domain size and phase separation between components.[20,30] Comparing *P(E,T)* values under short conditions, we found that the *P(E,T)* decayed in a manner similar to the domain growth tendency obtained using the GISAXS analysis (Fig. 4b and Fig. S10, ESI†). A little faster decrease of *P(E,T)* values compared with the domain size increase rates would originate from diverse factors that govern the 'burn-in' loss mechanism in OSCs, which has not yet been unveiled clearly and thus can be the focus of future investigation.[31] The $PC_{70}BM$ OSC showed a continuous *P(E,T)* reduction from 91.46% to 87.25% after 12 h and then to 76.31% after 7 days, while the ternary OSC was less affected. The *P(E,T)* of the ternary OSC started at 96.87% and remained relatively higher at 95.47% after 12 h and then 87.67% after 7 days of operation. It was notable that the *P(E,T)*

View Article Online
DOI: 10.1039/C9TA00382C

of 83.56% after 80 days of operation obtained from the ternary OSC exceeded that (<80%) of the $PC_{70}BM$ OSC after 1 day of operation.

Morphological transition simulation

The morphological changes in OSCs (which are closely correlated with both efficiency and stability) usually occur in two stages: local degradation followed by structural relaxation. This was also observed in our study, as will be discussed in the next section and shown in Fig. 6. As discussed in a recent paper by de Zerio and Müller,[32] this two-step relaxation process can be attributed to local nucleation and subsequent global growth of crystallization or glass formation of OSC components. Increasing the number of the OSC components provides similar kinetic and thermodynamic effects for both nucleation and growth rates. Kinetically, the decrease in diffusion coefficients of OSC components caused by incorporating additional components would lead to the delay of both nucleation and growth rates. Thermodynamically, adding additional components in OSCs would increase the entropy of mixing, which favours a homogeneous mixture over phase separation. This also plays a role in reducing both nucleation and growth rates of crystallization or glass formation of OSC components. Hence, understanding the molecular mechanism of the slowdown in the local nucleation process of crystallization or glass formation of OSC components upon increasing the number of components in OSCs would also provide significant insights into the long-term stability of ternary OSCs over the corresponding binary OSCs. In this spirit, we conducted molecular dynamics (MD) simulations using atomistic models of the three OSC systems to gain further insight into the relatively morphology evolution of OSCs. The atomistic MD simulations have been used to obtain insights into molecular packing behaviour in mixed regions of ternary blend films.[33] However, the MD simulations have intrinsic limitations in both time and length scales.[34] We thus focused on local morphological changes during the solvent evaporation process (see Figs. 5a-c), which were manifested by the change in the contact number between components. The model setup, including force field parameterization and simulation details, are presented in Experimental and Supplementary Method (ESI†).

The number of contacts between the same OSC components (PTB7-Th, $PC_{70}BM$ and ITIC-Th) was first calculated as a function of the simulation time during the solvent evaporation process. Here, the number of contacts was counted whenever the distance between any heavy atom pair in molecules (*A* and *B*) was less than a cut-off distance (r_c), and the r_c was set to 0.5 nm, 2.5 times the Lennard-Jones diameter of the carbon atom pair (0.20 nm).[35] Figs. 5d-f show the number of contacts per molecule between the identical components (PTB7-Th, $PC_{70}BM$, and ITIC-Th), which represent local morphological changes for the three OSC system, respectively. It should be noted that time zero in the simulation was set to the time right after the first 10% of solvents were removed from the systems. As expected, the contact number between each molecule increases with simulation time. However, the rate of the contact number is distinctive at each OSC system, and this result provides several interesting points worth mentioning. The number of contacts (N_c) between PTB7-Th was somewhat independent of the system composition (e.g., binary or ternary blends), showing similar contact number rates for each OSC system according to the simulation time (Fig. 5d). This result implies that the aggregation of PTB7-Th was not significantly influenced by the other OSC components. The number of contacts between PTB7-Th increased almost cubically with time ($\sim t^3$), indicating the polymeric nature of PTB7-Th. Importantly, the rates of contact number, v_c ($=dN_c/dt$), for both $PC_{70}BM$ and ITIC-Th became much slower in the ternary system than in the binary system. For instance, the rate of contact number for the $PC_{70}BM$ molecule was 2.90 ± 0.12 ns^{-1} in the binary PTB7-Th:$PC_{70}BM$ system and 1.31 ± 0.05 ns^{-1} in the ternary PTB7-Th:$PC_{70}BM$:ITIC-Th system, showing 55% (= (1 – (1.31/2.90)) × 100) retardation in the rate of contact number (Fig. 5e). However, this rate could also be influenced by the molecule concentration (ρ) in the system as $v_c \propto \rho D$, where D is the diffusion coefficient. The concentration reduction was calculated from the number, N, of $PC_{70}BM$ molecules in the two systems as: $\Delta\rho/\rho_{binary} = 1 - (\rho_{ternary}/\rho_{binary}) \approx 1 - (N_{ternary}/N_{binary}) = 1 - (105/172) = 0.39$. Even considering the 39% reduction of $PC_{70}BM$ concentration between the two systems, the 55% retardation in the rate of contact number was dramatic. This behaviour of $PC_{70}BM$ was in stark contrast with that of ITIC-Th, which showed a 53% decrease in v_c and a 58% decrease in ρ when comparing the ternary system with the corresponding binary system (PTB7-Th:ITIC-Th) (Fig. 5f). This indicates that the improved stability of the ternary system was mainly due to the decrease in the aggregation rate of both $PC_{70}BM$ and ITIC-Th. In the case of ITIC-Th, the aggregation rate was closely correlated with its concentration. On the other hand, the aggregation rate of $PC_{70}BM$ was significantly affected by the presence of the additional OSC component (ITIC-Th) as well as its concentration. This is consistent with the argument made by Tsai and Yeh regarding a high-entropy alloy (HEA).[36] Since the nucleation and growth of a new phase require the cooperative diffusion of all elements so that phase boundaries can successfully migrate, the slow-moving element (ITIC-Th) becomes the rate-limiting factor that impedes the physical transformation. It is worth mentioning that further experimental investigation on kinetic and thermodynamic transitions of BHJ morphology can strengthen our theoretical expectations, utilizing advanced analysis techniques to define molecular miscibility of blend components such as scanning transmission X-ray microscopy (STXM) or resonant soft X-ray scattering (R-SoXS) as demonstrated in recent reports.[37-39]

Long-term stability

Figs. 6a-c compare the time-dependent photovoltaic parameters between $PC_{70}BM$ binary and ternary OSCs at 60 °C. Devices showed similar performance decay tendencies with two stages of an exponential decline in performance at an

View Article Online
DOI: 10.1039/C9TA00938C

early stage of operation following a gradual linear decay on a longer timescale.[40] The PCE decay was highly restrained in the ternary OSC in both exponential and linear periods compared with that of the binary counterpart. For instance, the ternary OSC retained 90.1% of its initial efficiency after 12 h (8.47%) and 66.1% after one week (6.21%), which were higher than 83.1% after 12 h (6.76%) and 57.3% after one week (4.66%) for the $PC_{70}BM$ OSC. Notably, PCE was sustained at 5.78% (61.5% of initial PCE) after 30 days of operation, which even overwhelmed the 5.39% of $PC_{70}BM$ OSC only after 1 day of operation. The PCE loss behaviour under the thermal conditions (i.e., J_{SC} and fill factor (FF) reductions with almost constant open-circuit voltage (V_{OC})) (Fig. S11, ESI†) can be mainly attributed to coarsening of the morphology and phase separation between donor and acceptor materials according previous reports.[5,41] Therefore, we could designate the improved morphological stability in the ternary blend as a main factor for better performance retention in the corresponding ternary OSC during operation. We noted that the ternary OSC exhibited better stability compared with the ITIC-Th binary OSC, which proves the superiority of the ternary system in consistence with the theoretical expectations (Fig. S12, ESI†). A significant PCE drop was not observed in the ternary OSCs under the photo-induced degradation conditions (continuous AM 1.5G illumination, 100 $mWcm^{-2}$), suggesting the prospects of ternary OSCs in outdoor applications (Fig. S13, ESI†).[5] More insights into the photo-stability of non-fullerene acceptors in ternary systems will be the focus of future investigation.

Considering that PCE decreases linearly over long timescales, we assumed that there would be no critical drop in PCE for long-term operation and obtained a PCE of ~4.67% after one year of operation by extrapolating the experimentally obtained PCE for 193 days (Fig. 6d). The lifetime of the ternary OSC (defined by the point at which the PCE dropped by 20% from the start of the linear decay period) was estimated to be around ~490 days under the constant thermal condition, which was almost twice as long as the ~250 days obtained from the $PC_{70}BM$ OSC.[40] These indicate that ternary blends containing fullerene and non-fullerene acceptors benefit from combined optoelectronic properties of both kinds of acceptor materials as well as suppressed domain growth via kinetic and thermodynamic effects during operation, resulting in OSCs with enhanced efficiency and extended lifetimes. This morphological stability was theoretically supported by MD simulations using the atomistic models of the ternary system.

Conclusions

In summary, we utilized a non-fullerene acceptor, ITIC-Th, in conventional polymer:fullerene blends as a platform for ternary OSCs with high efficiency and long-term stability. ITIC-Th played important roles as a charge cascade acceptor and morphology controller to improve charge separation and transport process in the ternary OSC. Morphology evolution simulation also showed that the slow-moving component ITIC-Th controls the time-scale of the morphological change by slowing down the domain growth of the ternary OSC. The combined results of theoretical expectations and experimental measurements showed that the ternary OSC had improved stability by suppressing domain growth and arresting the optimized morphology under real operational conditions. Therefore, the ternary OSC exhibited significantly increased device lifetimes with better resistance to performance decay on a long timescale compared with the conventional binary OSCs. We believe this prototypical study opens new possibilities for non-fullerene acceptors to achieve high-efficiency optoelectronic devices in conjunction with commercially acceptable long-term stability.

Experimental

OSC fabrication

OSCs were fabricated using an inverted device structure of indium tin oxide (ITO)/poly[(9,9-bis(3'-(*N*,*N*-dimethylamino)propyl)-2,7-fluorene)-*alt*-2,7-(9,9-dioctylfluorene) (PFN)/active layer/MoO_3/Ag. PTB7-Th (1-material), $PC_{70}BM$ (Nano-C), and ITIC-Th (1-material) were mixed (1:*x*:1.5-*x*, $0 \le x \le 1.5$) in chlorobenzene/CN (98/2 vol/vol) with a total concentration of 25 mg ml^{-1} and were then magnetically stirred at 50 °C for 12 h. The blend solution was spin-coated atop an ultrathin PFN layer (~5 nm) on an ITO-glass substrate in a glove box filled with Ar, followed by drying at room temperature overnight. The experimentally optimized active layer thicknesses were 95, 120, and 105 nm for $PC_{70}BM$ binary, ITIC-Th binary, and ternary devices, respectively (Fig. S14, ESI†). An 8-nm-thick MoO_3 layer and a 100-nm-thick Ag layer were thermally evaporated in a vacuum chamber at $<10^{-7}$ Torr. The fabrication process was completed by sealing the devices using encapsulation glass and UV-curable epoxy.

OSC characterization

J–*V* characteristics of the OSCs were obtained using a source meter (Keithley 2400, Tektronix) under an irradiance of 100 $mWcm^{-2}$ provided by a solar simulator (K201 LAB55, McScience). The light intensity was calibrated with a Si reference cell (K801S-K058, McScience). EQE spectra were measured using a spectral solar cell QE test system (K3100, McScience), and the EQE-derived J_{SC} was used to confirm the J_{SC} obtained from the *J*–*V* curves. The electron mobility of the devices was determined from *J*–*V* characteristics of electron-only devices (ITO/PFN/active layer/Al) fitted using the Mott-Gurney SCLC model.[42] The nanoscale blend morphology was observed using tapping-mode AFM (XE-100, Park Systems). For the long-term stability test, the *J*–*V* characteristics of encapsulated devices were measured under AM 1.5G illumination with repeated cycles of dark thermal heating at 60 °C and device testing at room temperature.

GISAXS analysis

GISAXS measurements were performed at the 3C beam line of the Pohang Accelerator Laboratory, Republic of Korea. In the morphological stability test, the encapsulated samples were thermally treated at 60 °C on a pre-heated digital hotplate in dark ambient conditions for 12 h or 7 days. The 1D in-plane GISAXS scattering intensity was model-fitted with the following equation: $I(Q) = P(Q)S(Q) + b$, in which $P(Q)$ is related to the form factor of the particles, $S(q)$ is the fractal structure factor describing the interaction between particles in this fractal-like aggregation system, and b is the background scattering factor. We obtained the domain size using the correlation length (ξ) of the fractal-like aggregates according to the previous literature.[43-45]

MD Simulations

Atomistic molecular models for binary PTB7-Th:$PC_{70}BM$, binary PTB7-Th:ITIC-Th, and ternary PTB7-Th:$PC_{70}BM$:ITIC-Th blend systems were built up using the CHARMM General Force Fields (CGenFF version 3.0.1).[46,47] We followed the general parameterization scheme given by the CGenFF program to parameterize the force fields for the OSC systems.[48,49] Further details related to the analyses of the OSC systems from the MD simulations can be found in Supplementary Method (ESI†).

Conflicts of interest

There are no conflicts to declare.

Acknowledgements

This research was supported by Basic Science Research Program and Pioneer Research Center Program through the National Research Foundation of Korea, which is funded by the Ministry of Science, ICT, and Future Planning (NRF-2016R1C1B2014644, NRF-2016M3C1A3909138, NRF-2015R1A5A1009962), and by the Energy Technology Development Program of the Korea Institute of Energy Technology Evaluation and Planning (KETEP) grant (No.20163010012570) funded by the Korean government.

References

1 Z. He, B. Xiao, F. Liu, H. Wu, Y. Yang, S. Xiao, C. Wang, T. P. Russell and Y. Cao, *Nat. Photon*ics, 2015, **9**, 174.
2 J. K. Lee, W. L. Ma, C. J. Brabec, J. Yuen, J. S. Moon, J. Y. Kim, K. Lee, G. C. Bazan and A. J. Heeger, *J. Am. Chem. Soc*., 2008, **130**, 3619.
3 Z. He, C. Zhong, S. Su, M. Xu, H. Wu and Y. Cao, *Nat. Photonics*, 2012, **6**, 591.
4 L. Lu, T. Xu, W. Chen, E. S. Landry and L. Yu, *Nat. Photonics,* 2014, **8**, 716.
5 M. Nam, M. Cha, H. H. Lee, K. Hur, K.-T. Lee, J. Yoo, I. K. Han, S. J. Kwon and D.-H. Ko, *Nat. Commun.,* 2017, **8**, 14068.
6 M. Jørgensen, K. Norrman and F. C. Krebs, *Sol. Energy Mater. Sol. Cells*, 2008, **92**, 686.
7 H. Zhong, X. Yang, B. deWith and J. Loos, *Macromolecules,* 2006, **39**, 218.
8 H.-W. Liu, D.-Y. Chang, W.-Y. Chiu, S.-P. Rwei and L. Wang, *J. Mater. Chem*., 2012, **22**, 15586.
9 W. Zhao, D. Qian, S. Zhang, S. Li, O. Inganäs, F. Gao and J. Hou, *Adv. Mater.,* 2016, **28**, 4734.
10 T. Liu, X. Xue, L. Huo, X. Sun, Q. An, F. Zhang, T. P. Russell, F. Liu and Y. Sun, *Chem. Mater.,* 2017, **29**, 2914.
11 Y. Lin, F. Zhao, Q. He, L. Huo, Y. Wu, T. C. Parker, W. Ma, Y. Sun, C. Wang, D. Zhu, A. J. Heeger, S. R. Marder and X. Zhan, *J. Am. Chem. Soc*., 2016, **138**, 4955.
12 W. Zhao, S. Li, H. Yao, S. Zhang, Y. Zhang, B. Yang and J. Hou, *J. Am. Chem. Soc*., 2017, **139**, 7148.
13 M. Drees, H. Hoppe, C. Winder, H. Neugebauer, N. S. Sariciftci, W. Schwinger, F. Schäffler, C. Topf, M. C. Scharber, Z. Zhu and R. Gaudiana, *J. Mater. Chem.,* 2005, **15**, 5158.
14 Y.-J. Cheng, C.-H. Hsieh, P.-J. Li and C.-S. Hsu, *Adv. Funct. Mater.,* 2011, **21**, 1723.
15 H.-W. Liu, D.-Y. Chang, W.-Y. Chiu, S.-P. Rwei and L. Wang, *J. Mater. Chem.,* 2012, **22**, 15586.
16 C. Lindqvist, J. Bergqvist, C.-C. Feng, S. Gustafsson, O. Bäcke, N. D. Treat, C. Bounioux, P. Henriksson, R. Kroon, E. Wang, A. Sanz-Velasco, P. M. Kristiansen, N. Stingelin, E. Olsson, O. Inganäs, M. R. Andersson and C. Müller, *Adv. Energy Mater.,* 2014, **4**, 1301437.
17 C. Wang, X. Xu, W. Zhang, S. B. Dkhil, X. Meng, X. Liu, O. Margeat, A. Yartsev, W. Ma, J. Ackermann, E. Wang and M. Fahlman, *Nano Energy*, 2017, **37**, 24.
18 T. Zhang, X. Zhao, D. Yang, Y. Tian and X. Yang, *Adv. Energy Mater.,* 2017, **8**, 1701691.
19 L. Lu, W. Chen, T. Xu and L. Yu, *Nat. Commun.,* 2015, **6**, 7327.
20 V. D. Mihailetchi, L. J. A. Koster, J. C. Hummelen and P. W. M. Blom, *Phys. Rev. Lett.,* 2004, **93**, 216601.
21 V. D. Mihailetchi, H. X. Xie, B. de Boer, L. J. A. Koster and P. W. M. Blom, *Adv. Funct. Mater.,* 2006, **16**, 699.
22 J.-L. Wu, F.-C. Chen, Y.-S. Hsiao, F.-C. Chien, P. Chen, C.-H. Kuo, M. H. Huang and C.-S. Hsu, *ACS Nano,* 2011, **5**, 959.
23 Z. He, C. Zhong, X. Huang, W.-Y. Wong, H. Wu, L. Chen, S. Su and Y. Cao, *Adv. Mater.,* 2011, **23**, 4636.
24 I. Riedel, J. Parisi, V. Dyakonov, L. Lutsen, D. Vanderzande and J. C. Hummelen, *Adv. Funct. Mater.,* 2004, **14**, 38.
25 J. Zhang, Y. Zhao, J. Fang, L. Yuan, B. Xia, G. Wang, Z. Wang, Y. Zhang, W. Ma, W. Yan, W. Su and Z. Wei, *Small,* 2017, **13**, 1700388.
26 F. Liu, W. Zhao, J. R. Tumbleston, C. Wang, Y. Gu, D. Wang, A. L. Briseno, H. Ade and T. P. Russell, *Adv. Energy Mater.,* 2014, **4**, 1301377.
27 J. Zhang, Y. Zhang, J. Fang, K. Lu, Z. Wang, W. Ma and Z. Wei, *J. Am. Chem. Soc.,* 2015, **137**, 8176.
28 P. Bi, F. Zheng, X. Yang, M. Niu, L. Feng, W. Qin and X. Hao, *J. Mater. Chem. A,* 2017, **5**, 12120.
29 Y.-J. Hsieh, Y-C. Huang, W.-S. Liu, Y.-A. Su, C.-S. Tsao, S.-P. Rwei and L. Wang, *ACS Appl. Mater. Interfaces,* 2017, **9**, 14808.
30 B. A. Collins, Z. Li, J. R. Tumbleston, E. Gann, C. R. McNeil and H. Ade, *Adv. Energy Mater*., 2013, **3**, 65.
31 J. Kong, S. Song, M. Yoo, G. Y. Lee, O. Kwon, J. K. Park, H. Back, G. Kim, S. H. Lee, H. Suh and K. Lee, *Nat. Commun.*, 2014, **5**, 5688.
32 A. D. de Zerio and C. Müller, *Adv. Energy Mater*., 2018, 1702741.
33 Z. Wang, X. Zhu, J. Zhang, K. Lu, J. Fang, Y. Zhang, Z. Wang, L. Zhu, W. Ma, Z. Shuai and Z. Wei, *J. Am. Chem. Soc.*, 2018, **140**, 1549.
34 K. Do, M. K. Ravva, T. Wang and J.-L. Brédas, *Chem. Mater*., 2017, **29**, 346.
35 R. Alessandri, J. J. Unsitalo, A. H. de Vries, R. W. A. Havenith and S. J. Marrink, *J. Am. Chem. Soc.,* 2017, **139**, 3697.
36 M.-H. Tsai and J.-W. Yeh, *Mater. Res. Lett.,* 2014, **2**, 107.
37 L. Ye, W. Zhao, S. Li, S. Mukherjee, J. H. Carpenter, O. Awartani, X. Jiao, J. Hou and H. Ade, *Adv. Energy Mater.,* 2017, **7**, 1602000.

View Article Online
DOI: 10.1039/C9TA00382G

38 L. Ye, B. A. Collins, X. Jiao, J. Zhao, H. Yan and H. Ade, *Adv. Energy Mater.,* 2018, **8**, 1703058.
39 L. Ye, H. Hu, M. Ghasemi, T. Wang, B. A Collins, J.-H. Kim, K. Jiang, J. H. Carpenter, H. Li, Z. Li, T. McAfee, J. Zhao, X. Chen, J. L. Y. Lai, T. Ma, J.-L. Bredas, H. Yan and H. Ade, *Nat. Mater.,* 2018, **17**, 253.
40 C. H. Peters, I. T. Sachs-Quintana, J. P. Kastrop, S. Beaupré, M. Leclerc and M. D. McGehee, *Adv. Energy Mater.,* 2011, **1**, 491.
41 B. Ray, P. R. Nair and M. A. Alam, *Sol. Energy Mater. Sol. Cells,* 2011, **95**, 3287.
42 Z. He, C. Zhong, X. Huang, W.-Y. Wong, H. Wu, L. Chen, S. Su and Y. Cao, *Adv. Mater.,* 2011, **23**, 4636.
43 J. Teixeira, *J. Appl. Cryst.,* 1988, **21**, 781.
44 H.-C. Liao, C.-S. Taso, Y.-T. Shao, S.-Y. Chang, Y.-C. Huang, C.-M. Chuang, T.-H. Lin, C.-Y. Chen, C.-J. Su, U.-S. Jeng, Y.-F. Chen and W.-F. Su, *Energy Environ. Sci.,* 2013, **6**, 1938.
45 H.-J. Jhuo, S.-H. Liao, Y.-L. Li, P.-N. Yeh, S.-A. Chen, W.-R. Wu, C.-J. Su, J.-J. Lee, N. L. Yamada and U.-S. Jeng, *Adv. Funct. Mater.,* 2016, **26**, 3094.
46 K. Vanommeslaeghe, E. Hatcher, C. Acharya, S. Kundu, S. Zhong, J. Shim, E. Darian, O. Guvench, P. Lopes, I. Vorobyov and A. D. MacKerell Jr., *J. Comput. Chem.,* 2010, **31**, 671.
47 W. Yu, X. He, K. Vanommeslaeghe and A. D. MacKerell Jr., *J. Comput. Chem.,* 2012, **33**, 2451.
48 K. Vanommeslaeghe and A. D. MacKerell Jr., *J. Chem. Inf. Model.,* 2012, **52**, 3144.
49 K. Vanommeslaeghe, E. P. Raman and A. D. MacKerell Jr., *J. Chem. Inf. Model.,* 2012, **52**, 3155.

View Article Online
DOI: 10.1039/C9TA00382G

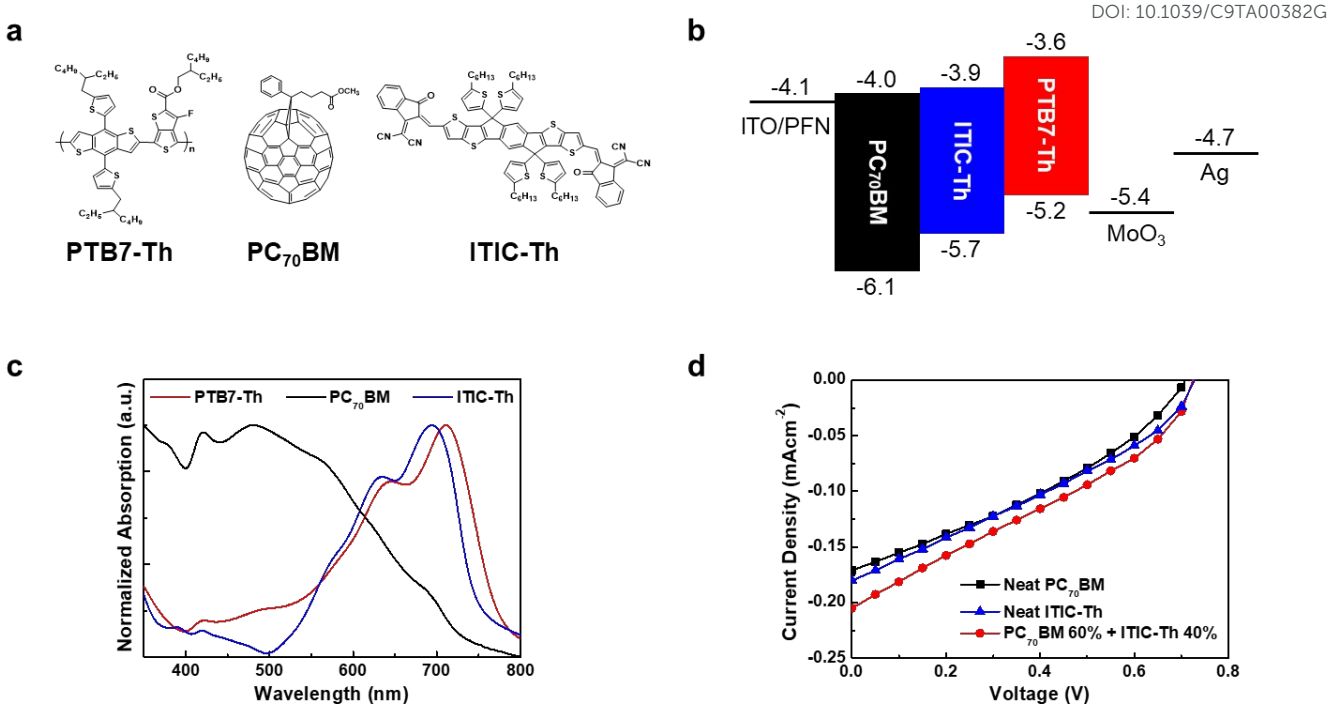

Fig. 1 Material properties. (a) Chemical structures, (b) energy levels, and (c) normalized UV-vis absorption spectra of PTB7-Th, $PC_{70}BM$, and ITIC-Th. (d) *J-V* characteristics of acceptor-only devices based on $PC_{70}BM$, ITIC-Th, and $PC_{70}BM$:ITIC-Th (60:40) blend films under AM 1.5G illumination (100 $mWcm^{-2}$).

View Article Online
DOI: 10.1039/C9TA00382G

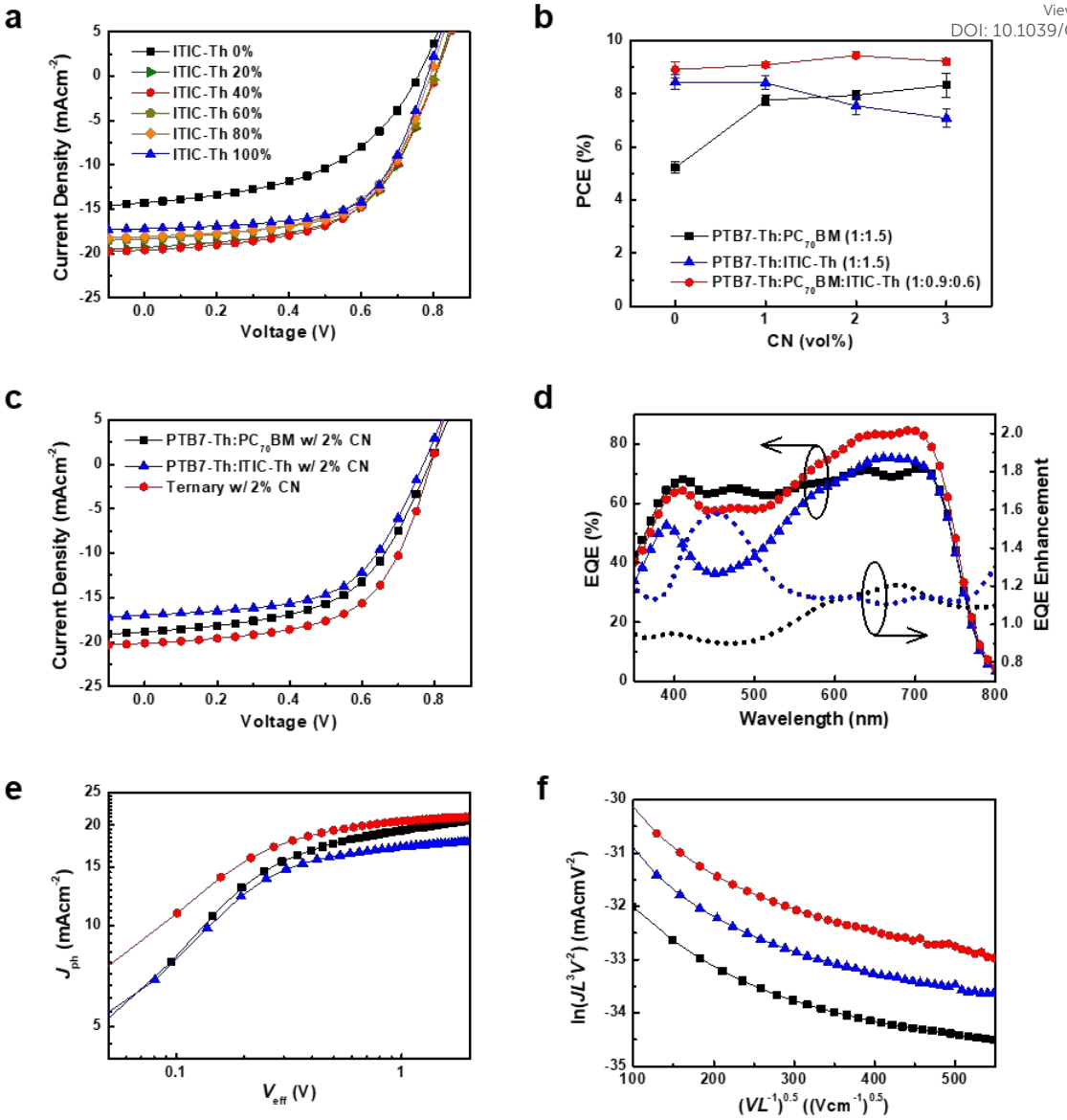

Fig. 2 Optimization and characterization of ternary OSCs. (a) Optimization of the ratio between $PC_{70}BM$ and ITIC-Th in the ternary OSCs without solvent additive. (b) PCE variation of $PC_{70}BM$ binary, ITIC-Th binary, and optimized ternary (ITIC-Th 40%) devices for different CN vol%. The average and standard deviation values in (b) were obtained from more than 10 devices. Comparison of photovoltaic characteristics between $PC_{70}BM$ binary, ITIC-Th binary, and ternary OSCs containing 2 vol% CN: (c) *J-V* characteristics, (d) EQE spectra and EQE enhancement ratios between devices, (e) J_{ph}-V_{eff} characteristics, and (f) SCLC electron mobility. The dotted lines in (d) indicate EQE enhancement ratio of the ternary OSC relative to the $PC_{70}BM$ (black dotted line) or ITIC-Th (blue dotted line) binary references.

View Article Online
DOI: 10.1039/C9TA00382G

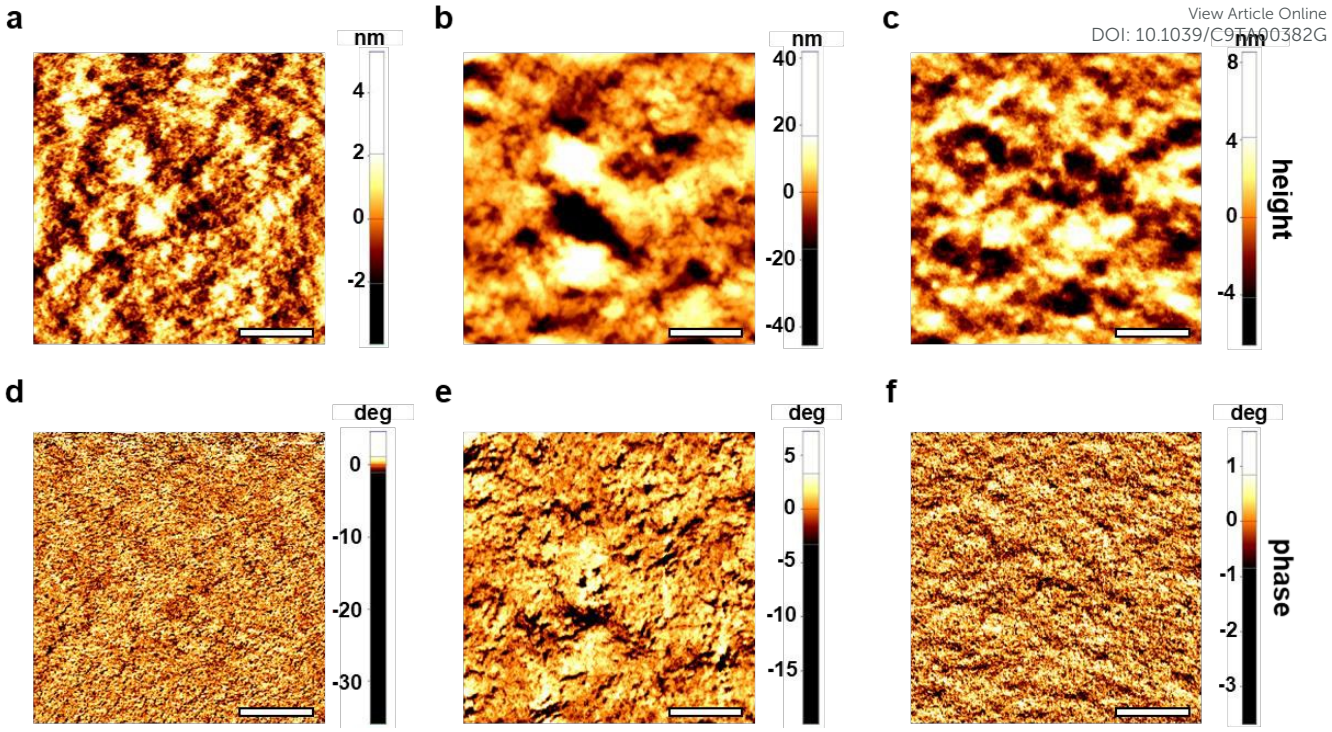

Fig. 3 Ternary blend morphology. AFM topography and phase images of (a, d) $PC_{70}BM$ binary, (b, e) ITIC-Th binary, (c, f) and ternary BHJ films, respectively. The scale bars indicate 500 nm, and the scan area is 2 × 2 μm^2.

View Article Online
DOI: 10.1039/C9TA00382G

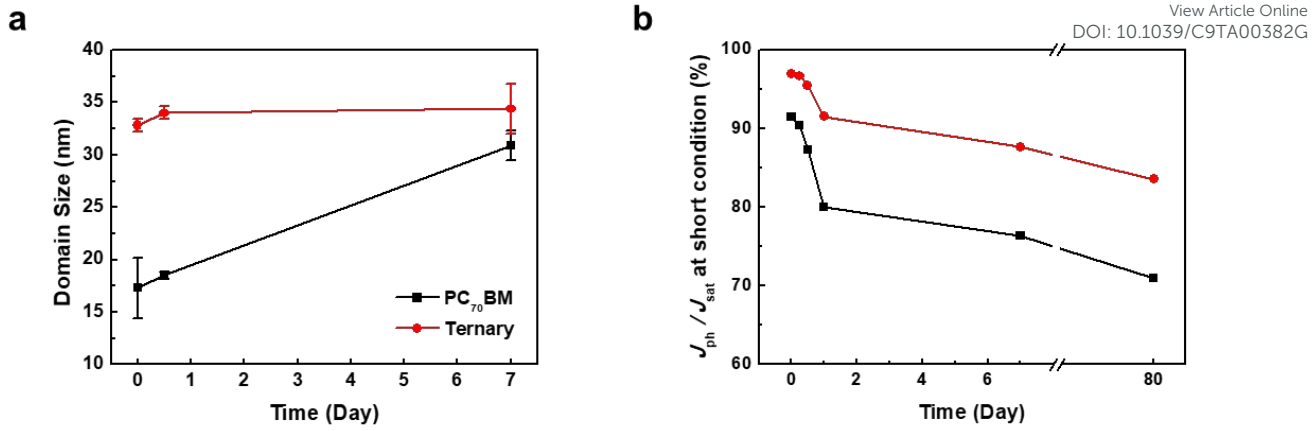

Fig. 4 Domain growth and charge transfer analysis. (a) GISAXS-derived overall domain size variation and (b) J_{ph}/J_{sat} values at a short-circuit condition of $PC_{70}BM$ binary and ternary blends for different annealing durations at 60 °C.

View Article Online
DOI: 10.1039/C9TA00382G

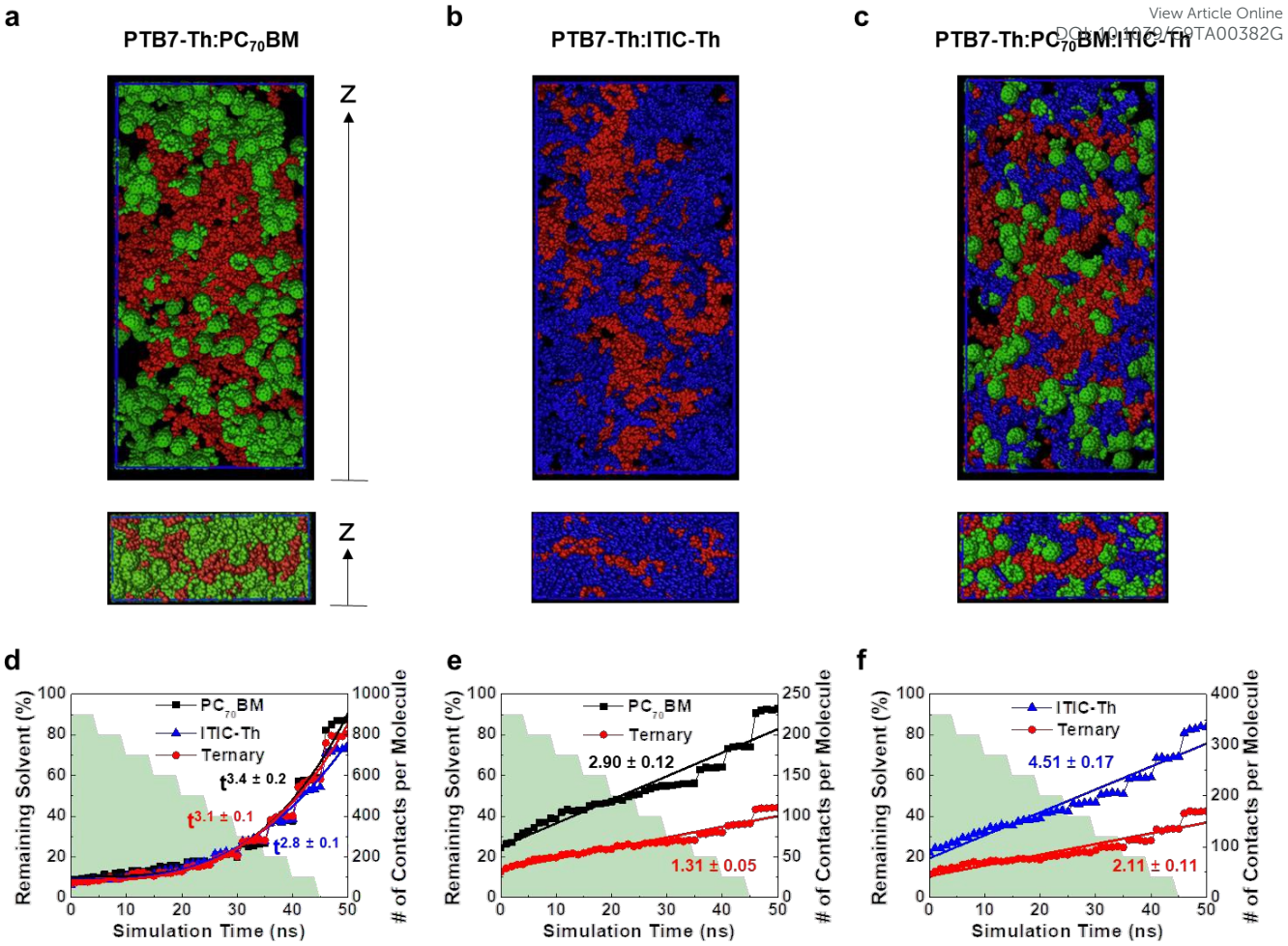

Fig. 5 Morphology evolution simulation. Side views before solvent evaporation (upper) and after 100% solvent evaporation (lower) for (a) $PC_{70}BM$ binary, (b) ITIC-Th binary, and (c) ternary OSCs. PTB7-Th, $PC_{70}BM$, and ITIC-Th are represented as red, green, and blue colours, respectively, and solvents are omitted for clarity. The number of contacts per molecule between the same OSC components: (d) PTB7-Th, (e) $PC_{70}BM$, and (f) ITIC-Th. In (d), the line and numbers correspond to the power fit, and the lines and numbers in (e) and (f) correspond to the slopes of the linear fit. The green bars in the background indicate the percentage of solvents remaining in the system.

View Article Online
DOI: 10.1039/C9TA00382G

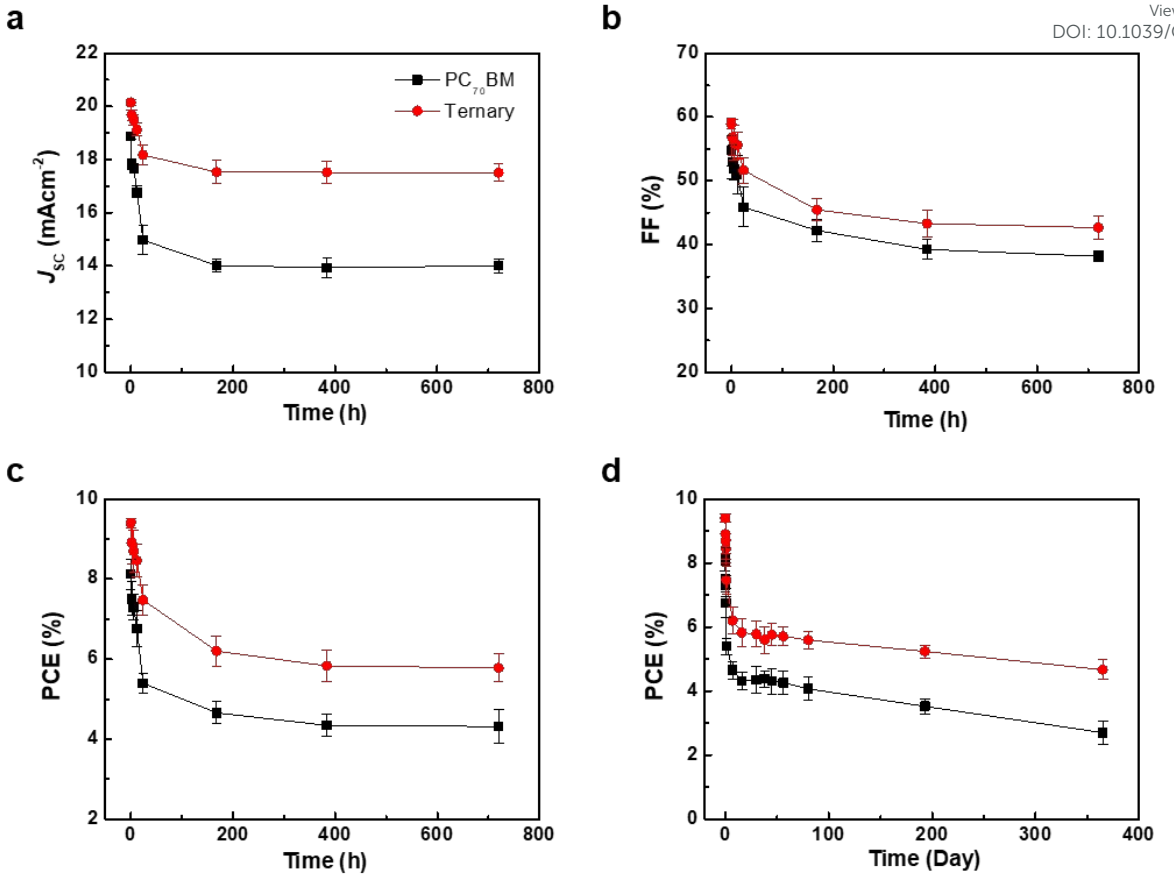

Fig. 6 Long-term stability test. Comparison of time-dependent photovoltaic parameters of $PC_{70}BM$ binary and ternary OSCs under thermal treatment at 60 °C: (a) J_{SC}, (b) FF, and (c) PCE. (d) Long-term PCE variation of the OSCs at 60 °C for 1 year obtained by extrapolating the experimentally obtained PCE values for 193 days. The average and standard deviation values were obtained from more than 8 devices.

View Article Online
DOI: 10.1039/C9TA00382G

We demonstrate the improved morphological stability and lifetime of ternary organic solar cells incorporating nonfullerene small molecules in polymer:fullerene blends.

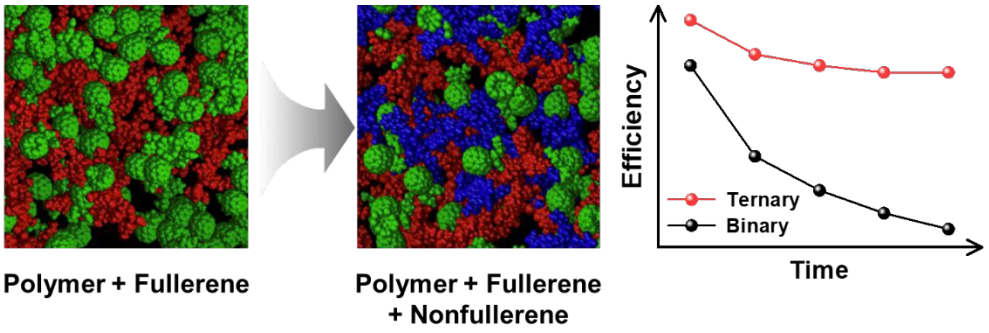

Keywords: Organic solar cell, Ternary blend, Stability, Non-fullerene acceptor, Morphology